



Marked coastal warming off Tokai attributable to Kuroshio large meander

Shusaku Sugimoto^{1,2} · Bo Qiu³ · Atsushi Kojima⁴

Received: 6 August 2019 / Revised: 20 September 2019 / Accepted: 10 October 2019
© The Oceanographic Society of Japan and Springer Nature Singapore Pte Ltd. 2019

Abstract

The Kuroshio takes a large meander (LM) path since summer of 2017 for the first time since the 2004–2005 event and is the sixth LM event since 1965. It has been commonly recognized that a cool water pool is distributed broadly in the inshore region between the Kuroshio and southern coast of the Tokai district, Japan, during the LM periods. By using the recently-developed 1-km high-resolution sea surface temperature data, here we show marked coastal warming off the Tokai district during the LM periods, despite the Kuroshio not passing through the coastal area. The archived temperature–salinity profiles reveal that large positive anomalies off the Tokai district exist not only at the sea surface but also below 300 m and the water properties of which are those of the offshore Kuroshio water. The warm, salty waters are transported inshore by the westward Kuroshio which bifurcates at around 138° E, 34° N, during the LM path periods. We detect an increased upward heat release via turbulent heat fluxes along the coastal warming region from the new-generation atmosphere reanalysis data on a 25 km grid. These are common features to the past LMs and, furthermore, the region around the Kanto-Tokai districts becomes warmer than usual in warm seasons during the LM events. Our result reveals that the LM event can exert an influence upon the Japanese climate via the coastal air–sea interaction.

Keywords Coastal warming off the tokai district · Japan · Physical oceanography · Kuroshio large meander · Satellite observations · Temperature–salinity profiles · Air–sea interaction · Air–sea heat exchange

1 Introduction

The Kuroshio is a warm western boundary current that transfers substantial amounts of heat from the western tropical Pacific to the mid-latitude region of the western North Pacific. It flows east-northeastward along the Pacific Ocean side of the Japanese islands and then veers off the Japanese coast to the east at around 35° N, forming the eastward jet known as the Kuroshio Extension (KE). Variations in Kuroshio's shape and position have a large influence on regional

fisheries, ship navigation, marine resources, etc. It has been known that the Kuroshio takes three typical paths south of Honshu, Japan: the large meander path (LM), the offshore nonlarge meander (NLM) path (oNLM), and the nearshore nonlarge meander path (nNLM) (Fig. 1a) (Kawabe 1995). These path features are considered to be related to the particular ocean bottom topography south of Honshu. Specifically, the Izu-Ogasawara Ridge has two major water gates: the LM and nNLM go through the northern gate, whereas the oNLM goes through the southern gate.

In the LM period, a developed cyclonic eddy is present in the inshore region between the Kuroshio and the southern coast of the Tokai district (Fig. 1c). It has been recognized that the cool water pool is distributed broadly due to the upwelling and the shoaling thermocline inside the cyclonic eddy (Fig. 1c). The LM-induced cool water pool can affect fisheries, such as a poor anchovy catch and changes in the fishing ground of bonito (NRIFS 2005), and the overlying atmosphere field in the terms of a reduction in surface wind speed and precipitation (Xu et al. 2010; Murazaki et al. 2015). Past works denoted that the warm Kuroshio water

✉ Shusaku Sugimoto
shusaku.sugimoto.d7@tohoku.ac.jp

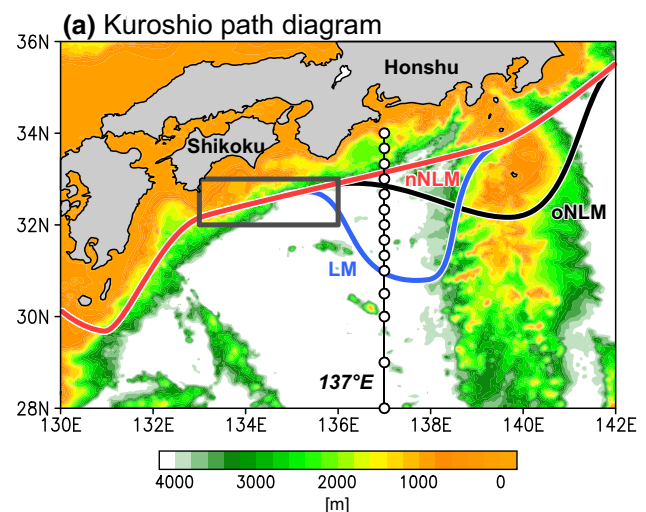
¹ Department of Geophysics, Graduate School of Science, Tohoku University, Sendai 980-8578, Japan

² International Pacific Research Center, University of Hawaii at Manoa, Honolulu, HI 96822, USA

³ Department of Oceanography, University of Hawaii Manoa, Honolulu, HI 96822, USA

⁴ Global Environment and Marine Department, Japan Meteorological Agency, Tokyo 100-8122, Japan

Fig. 1 **a** Three typical paths of the Kuroshio south of Japan based on Kawabe (1995): LM, nNLM, and oNLM. Shading denotes bathymetry features from the National Geophysical Data Center's 2-min gridded elevation/bathymetry for the world (ETOPO2; <https://www.ngdc.noaa.gov>) (m). Open circles show repeat hydrographic sections along 137° E, conducted by the Japan Meteorological Agency (JMA). Black rectangle represents a sea area off the Shikoku (32°–33° N, 133°–136° E). **b** Southernmost location (°N) of the Kuroshio between 136° and 140° E, produced by the JMA; the location is determined based on the temperature at a depth of 200 m and satellite-derived SST data. Red colors represent a main analysis period of this study. Shading denotes six LM periods since 1965, defined by the JMA: LM1 (August 2017–present), LM2 (July 2004–August 2005), LM3 (December 1989–December 1990), LM4 (December 1986–July 1988), LM5 (November 1981–May 1984), and LM6 (August 1975–March 1980). **c** SST in October 2017 (color), when the Kuroshio takes the LM path, from MURSST (see details in text). Black contour indicates satellite-derived sea surface height (SSH) (see detailed in text), with an interval of 0.2 m, in October 2017



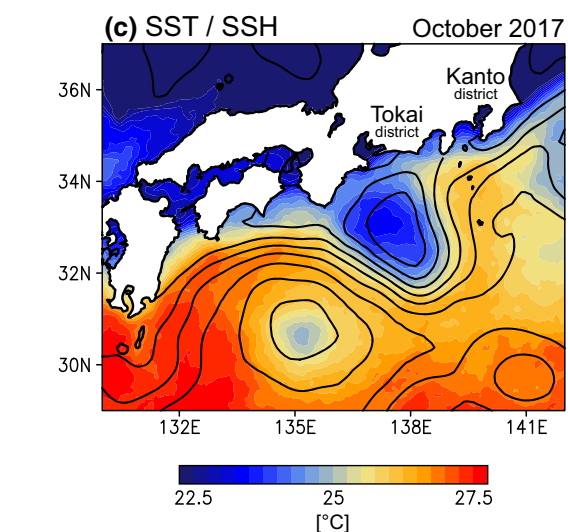
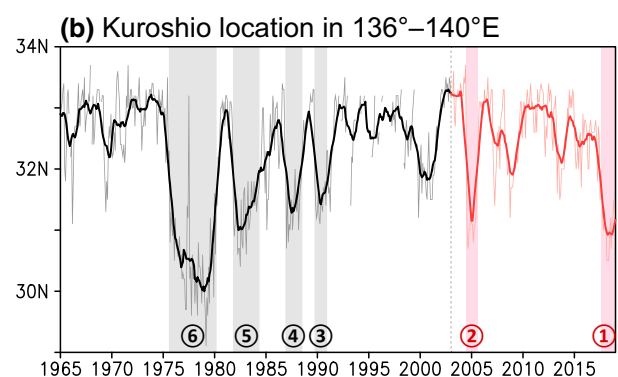
tends to intrude into the coastal area off the Tokai district from in-situ profiles during the LM paths (Okada 1977; Kasai et al. 1993; Nakata et al. 2000; Maximenko 2002), but its spatial features have not yet been clarified because of a lack of data.

In summer of 2017, the Kuroshio took the LM path for the first time since the summer of 2005 (Fig. 1b), and this event is still on-going in autumn of 2019. Recently, NASA Jet Propulsion Laboratory developed the multiscale ultra-high-resolution sea surface temperature (SST) (MURSST) product (Chin et al. 2013) with a horizontal resolution of 1 km, and ECMWF released the Fifth generation of atmospheric reanalysis of the global climate (ERA5; Copernicus Climate Change Service 2017) with a spatial resolution of 25 km. The availability of temperature-salinity profiles has also increased dramatically year by year since 2000 when the international Argo project (Argo Science Team 2001) started. These improved datasets provide us with a new perspective on the LM-induced SST. In this study, we investigate SST in the inshore region of the Kuroshio attributable to the LM path and then attempt to detect its cause using the latest datasets.

2 Data and processing procedures

We use the daily MURSST product (Chin et al. 2013). This incorporates SSTs from eight satellites, using both infrared and passive microwave retrievals, and in-situ data. It has been used previously for research on coastal upwelling (Vazquez-Cuervo et al. 2013; Gentemann et al. 2017). This product is available from January 2003 onward.

Monthly atmospheric variables of net surface heat flux (NHF; i.e., the sum of net surface longwave radiation, net surface shortwave radiation, latent heat flux, and sensible heat flux) and surface air temperature (SAT) are from the



ERA5 (Copernicus Climate Change Service 2017). The data have a $1/4^\circ$ (longitude) \times $1/4^\circ$ (latitude) spatial resolution and are available from 1979. We also use the monthly mean SAT data at weather stations and at the Automated Meteorological Data Acquisition System (AMeDAS) stations operated by JMA; most observations in the weather

stations began from 1960 and those in the AMeDAS station started in 1974.

We use temperature-salinity profiles archived in the *World Ocean Database 2018* (WOD18; Boyer et al. 2018) and at the Japan Oceanographic Data Center (JODC; available at <https://www.jodc.go.jp>), in a database compiled by the Japan Fisheries Research and Education Agency (FRA), and profiles from Argo floats (Oka et al. 2007). We performed data quality control, following a method of Sugimoto et al. (2017a). After quality control procedures, temperature-salinity profiles were vertically interpolated into 1-m intervals following Akima (1970). The Japan Meteorological Agency (JMA) conducts ongoing ship-based biannual (winter and summer) hydrographic surveys along 137° E (Fig. 1a). Stations along this line are located approximately 1/3° intervals in the Kuroshio region. We use statistically-analyzed temperature-salinity grid point values produced by the JMA (<https://www.data.jma.go.jp>).

We use Copernicus Marine Environment Monitoring Service (CMEMS; marine.copernicus.eu) sea surface height (SSH) product based on altimeter data from the satellites TOPEX/Poseidon, Jason-1, ERS-1/2, and Envisat, with daily temporal resolution and 1/4° (longitude) × 1/4° (latitude) spatial resolution. We use the information produced by the JMA for the Kuroshio path south of Japan; this has the 10-day temporal resolution. The axis is estimated comprehensively using data of ocean assimilation product (multivariate ocean variational estimation (MOVE) developed by the JMA/Meteorological Research Institute; Usui et al.

2006), satellite-derived SST image, and surface velocity data obtained by ship-borne acoustic Doppler current profilers (ADCP).

The main analysis period of this study is the 16 years from January 2003 to December 2018, when all dataset are available. We regard periods from July 2004 to August 2005 and from August 2017 onward as LM periods following the JMA (see red shadings in Fig. 1b) and periods for the consecutive 11 years of 2006 to 2016 as non-LM periods.

3 Results

3.1 Coastal warming off Tokai district in LM period

We explore spatial features of SST during the LM periods. In October 2017 when the Kuroshio takes the LM path, the negative SST anomalies are visible in the inshore region of the Kuroshio (Fig. 2a), as recognized previously. In addition, a closer look of the SST map reveals marked coastal warming off the Tokai to Kanto districts, which is 1–2 °C warmer than the non-LM periods. This coastal warming is detected throughout the LM periods both in the current and 2004–2005 events (Fig. 2b).

To check the relationship between the coastal warming and the LM paths, we examine SST patterns in the Kuroshio paths. Here, we define the nNLM and oNLM as follows: nNLM is located north of 32.5° N along 136° E, 33° N along 138° E, and 33.5° N along 140° E; and oNLM is

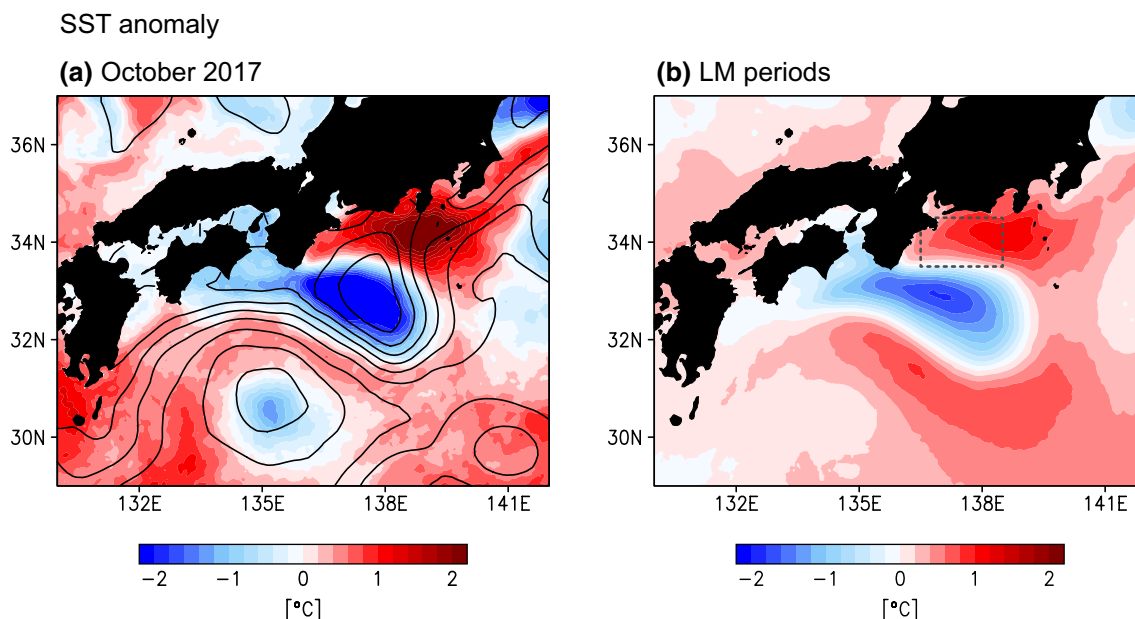
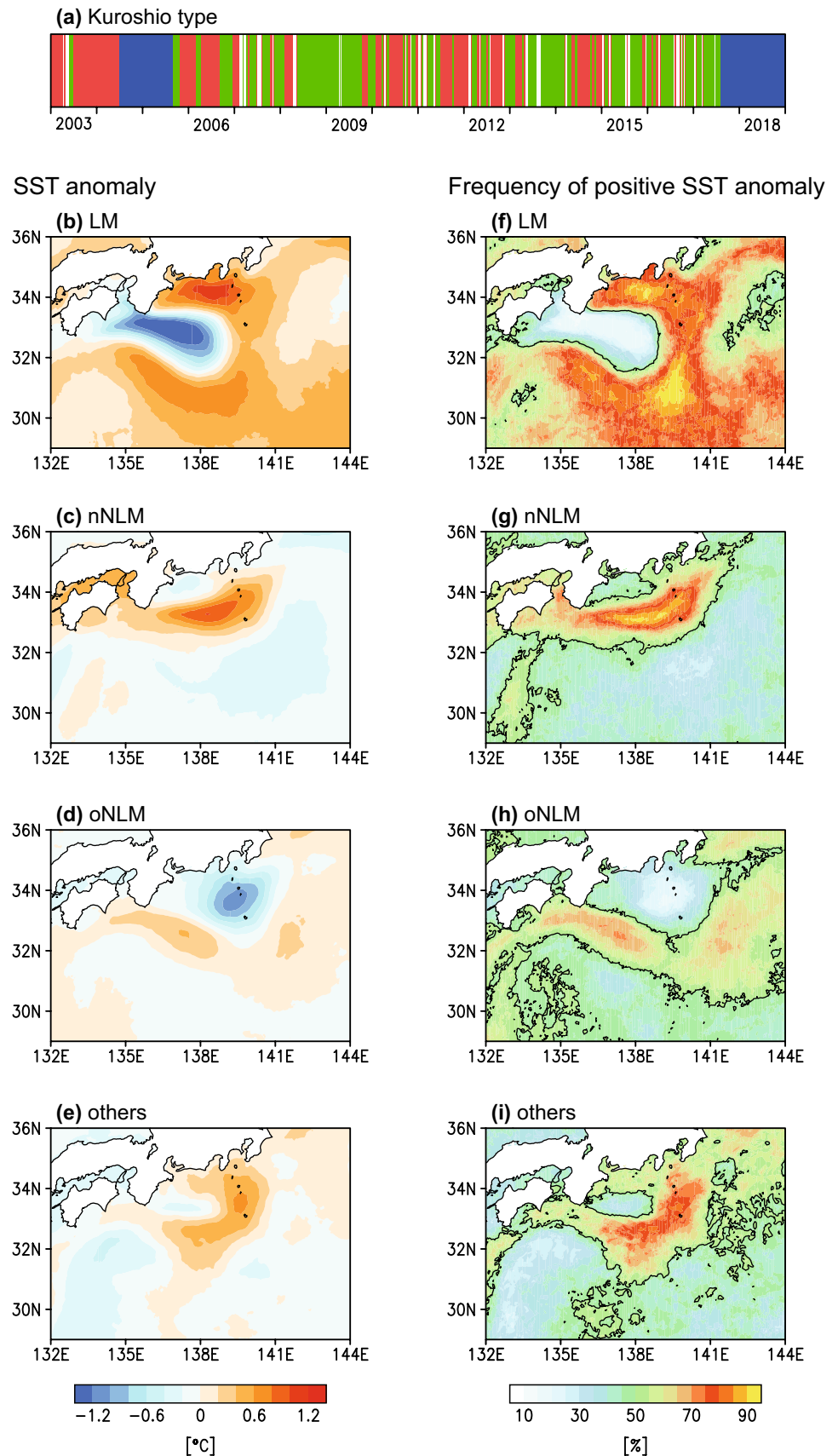


Fig. 2 **a** As in Fig. 1c, but for SST anomaly in October 2017; here, the monthly anomaly is different from monthly-mean SST during non-LM periods. **b** As in **a**, but for a composite map of monthly SST

anomaly during LM periods. A dashed rectangle represents CAT (33.5°–34.5° N, 136.5°–138.5° E)

Fig. 3 **a** Three-path period of the Kuroshio: blue, red, and green bars represent the LM, nNLM, and oNLM, respectively. Composite maps of 10-day SST anomaly in **b** LM, **c** nNLM, **d** oNLM, and **e** others; here, the daily anomaly is different from daily climatological data obtained by applying a 31-day running filter to calendar-day means throughout non-LM periods. **f** through **i** As in **b** through **e**, but for a frequency of positive SST anomaly. Black line represents 50% contour



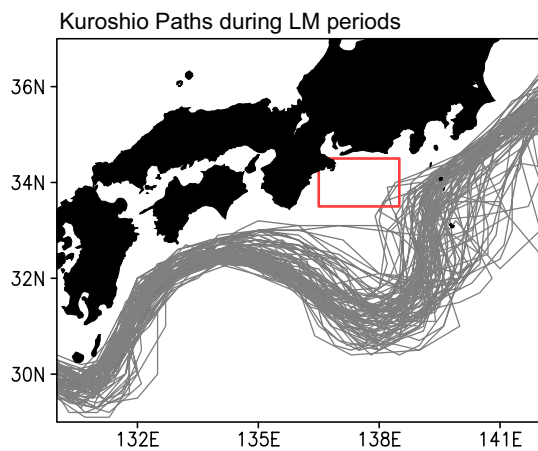


Fig. 4 The 10-day Kuroshio path, produced by JMA, during LM periods. Red rectangle represents CAT

situated south of 33.5° N along 140° E. Consequently, the days of paths for LM, nNLM, and oNLM are 1030 days (18%), 1820 days (32%), and 2320 days (40%), respectively (Fig. 3a). The remaining 590 days (10%) represent the transitioning paths of the Kuroshio, which we call the “others” paths. The coastal warming off the Tokai to Kanto districts is evident in LM paths (Fig. 3b), the warming of which occurs over 80–90% of the LM periods (Fig. 3f). On the other hand, the coastal warming is not detected in oNLM paths (Fig. 3d, h). In nNLM (Fig. 3c, g), although warming occurs off the Kanto district frequently, negative SST anomalies are observed at the coastal areas off the Tokai district.

Transitioning paths (Fig. 3e, i) display the coastal warming, especially large off the Kanto district, but its amplitude and frequency are considerably smaller compared to those in LM paths. The composite results shown in Fig. 3 reveal that the LM paths are related strongly to the coastal warming off the Tokai to Kanto districts, and the warming is particularly intense off the Tokai district.

3.2 Influence of westward Kuroshio bifurcation on coastal warming off the Tokai district

We focus in this subsection on the coastal area of the Tokai district (CAT; 33.5°–34.5° N, 136.5°–138.5° E; dashed rectangle in Fig. 2b) and investigate causes of the coastal warming. Figure 4 displays the Kuroshio paths during the LM periods. The Kuroshio which has flowed northward west of the Izu-Ogasawara Ridge approaches the coastal areas of the Kanto district and veers eastward in the nearshore areas. It is reasonable to hypothesize that the coastal warming off the Kanto district is mainly formed by the nearshore Kuroshio paths. However, the Kuroshio axis does not pass through the coastal area of the Tokai district during the LM periods, indicating a small direct influence of the Kuroshio on the warming in CAT.

What atmospheric or oceanic processes, except for the direct influence of the Kuroshio, contribute to the formation of coastal warming in CAT? To address this question, we examine the relationship between the NHF and SST in spatial features. In general, the NHF south of Honshu has clear seasonal changes; upward heat release in a form of latent

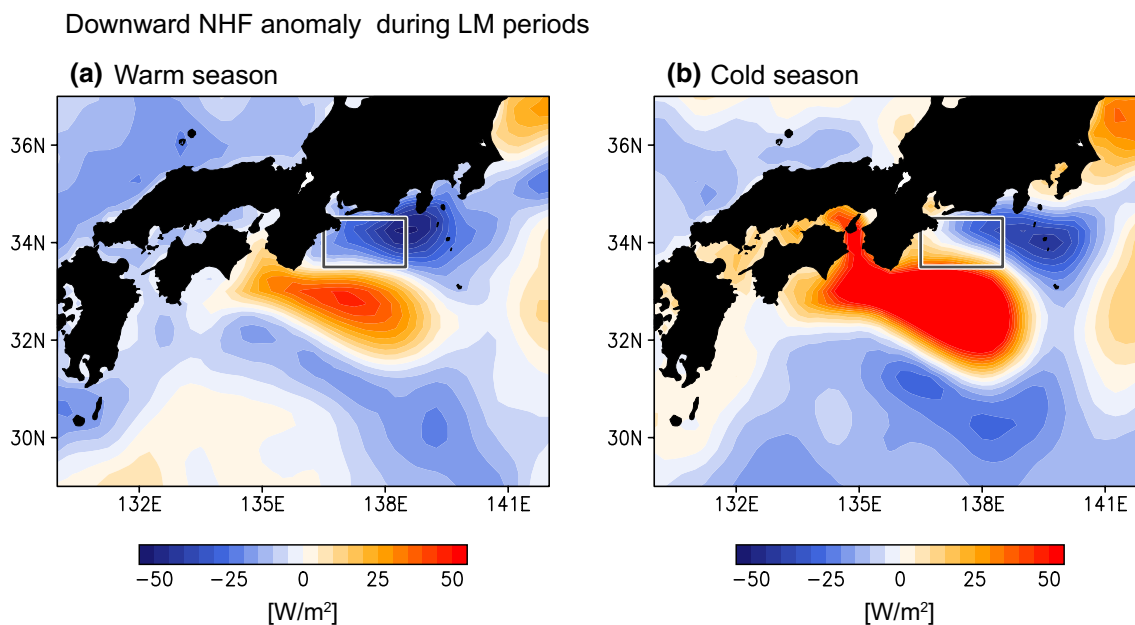


Fig. 5 As in Fig. 2 b, but for downward NHF anomaly in **a** warm season (May–October) and **b** cold season (November–April). Black rectangle represents CAT

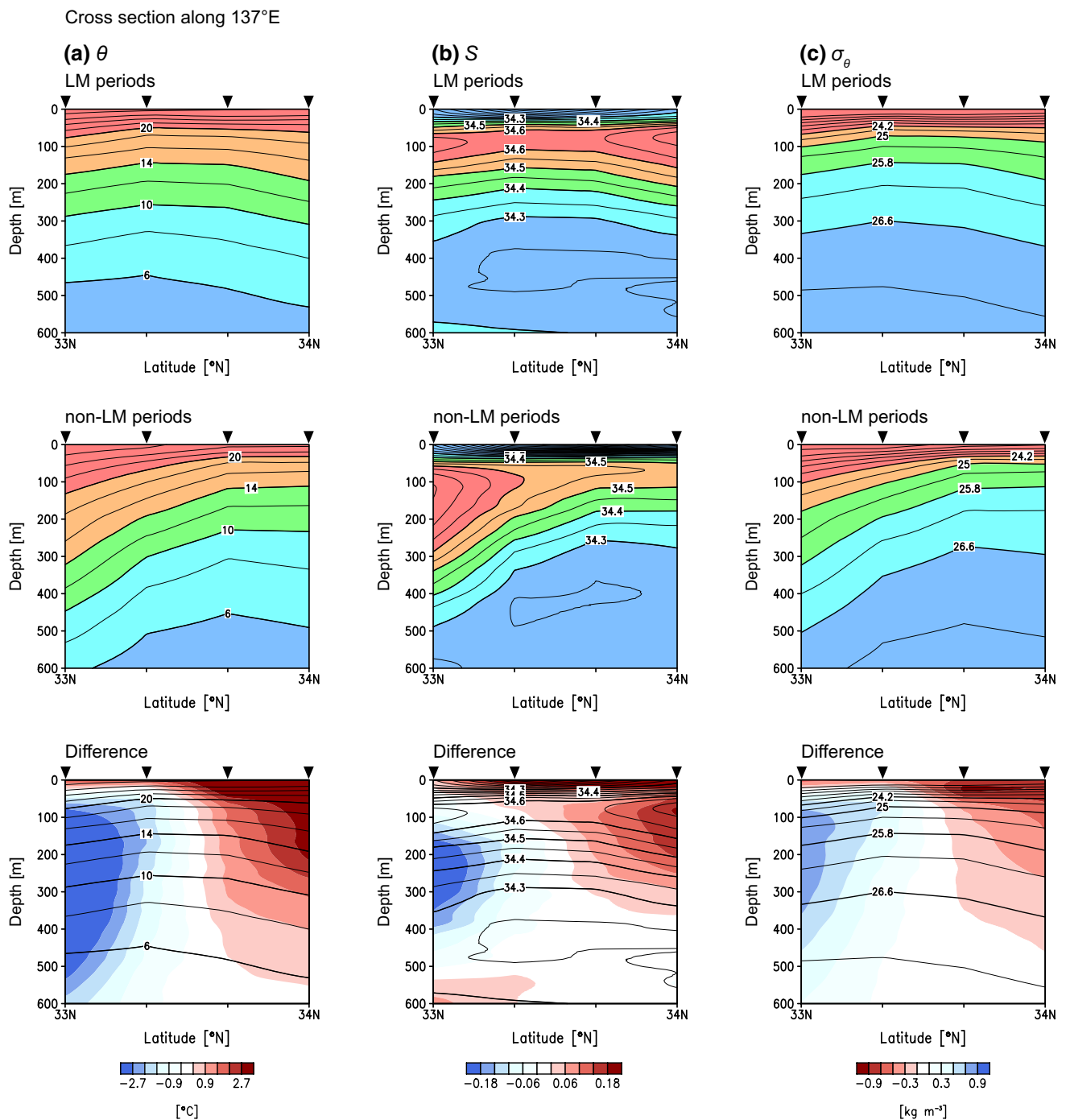


Fig. 6 Meridional cross sections at 137° E of **a** θ ($^{\circ}\text{C}$, contour interval is 2°C), **b** S (contour interval is 0.05), and **c** σ_{θ} (kg m^{-3} ; contour interval is 0.4 kg m^{-3}) from summer cruises along 137°E of (top) LM periods and (middle) non-LM periods, or (bottom) the difference

between the two periods (shading; contours indicate values in LM periods). Inverted triangles at the top of the panel indicate observation stations

and sensible heat flux in a cold season and downward solar heating in a warm season (e.g., Qiu et al. 2004). We perform a composite analysis of NHF for the two seasons during the LM periods. The NHF anomalies in both the warm and cold seasons (Fig. 5) have a clear tri-pole pattern south of

Honshu. Furthermore, the patterns bear a good resemblance to the sign-reversed pattern of SST in Fig. 2b, indicating that the SST tends to increase when the heat is released from the ocean to the overlying atmosphere and vice versa. This shows that the SST anomalies in CAT are not formed

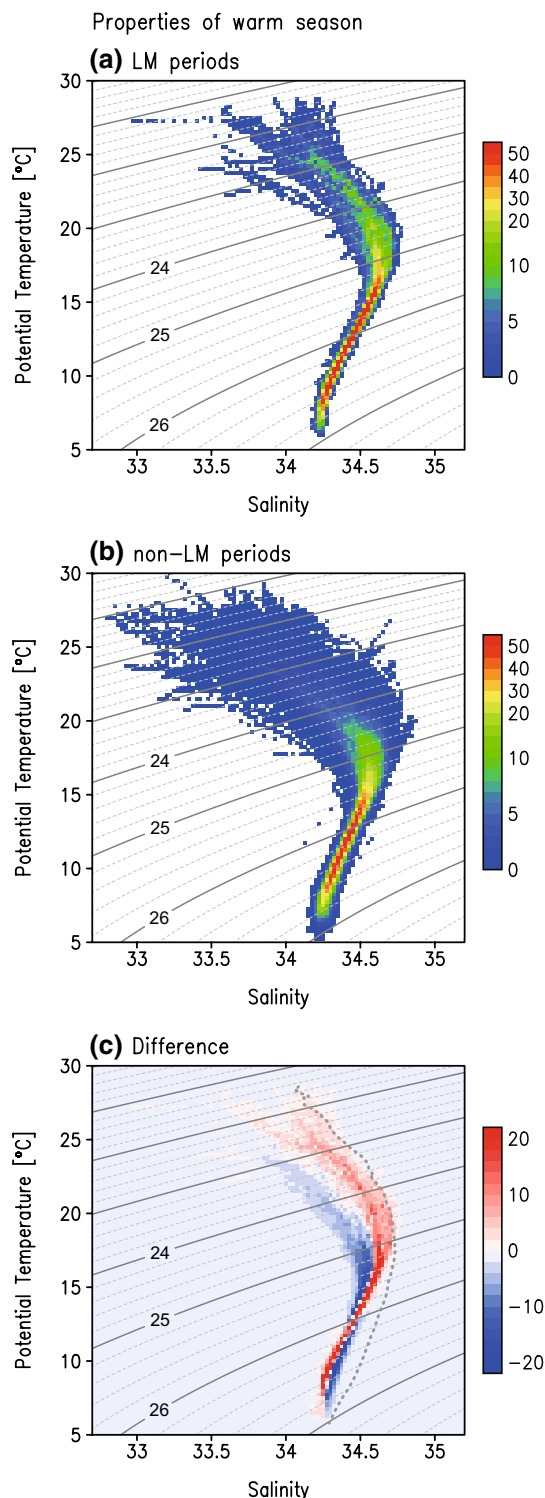


Fig. 7 Proportion of number of profiles from sea surface to 400 m in CAT of warm season (May–October) during **a** LM periods and **b** non-LM periods (%), as a function of temperature and salinity. Each number is 124 in LM periods and 1014 in non-LM periods. **c** Difference between the two periods (shading). Black dashed line indicates an isopycnal-mean profile for pure Kuroshio water off the Shikoku (black rectangle in Fig. 1a) during warm season of 2003–2018

through heat exchange between the ocean and atmosphere, but predominantly through oceanic processes.

Regarding the oceanic processes, we first investigate the ocean vertical structure to understand a possible cause of the CAT warming by using the 137° E repeat hydrographic sections. The previous LM event started in summer of 2004 and ended in summer of 2005, and the current LM started in summer of 2017 (red shadings in Fig. 1b). We specifically focus on summer sections (Fig. 6). A comparison of the two periods clearly shows that, in LM periods, the region north of 33.5° N is warmer (> 1.5 °C), saltier (> 0.1), and lighter (< 0.3 kg m⁻³) than non-LM periods, not only at the sea surface but also below 300 m (bottom panel in Fig. 6). The region north of 33.5° N along 137° E is inclusive in our defined CAT box. To confirm the results based on the 137° E hydrographic data, we examine whether the warmer–saltier water is distributed within CAT during the LM periods using the archived temperature–salinity profiles. The θ – S properties between the two periods are different evidently (Fig. 7); CAT is occupied by warm–salty water during the LM period. It is expected that the warm–salty water originates from the offshore water, i.e., the Kuroshio. We investigate the pure Kuroshio water, which is obtained from θ and S in an open area of the Shikoku where the Kuroshio passes regardless of its path types (see Fig. 1a). Here we use profiles of $\theta = 14$ – 16 °C at 200 m for the pure Kuroshio water, as the axis of the Kuroshio can be defined by the $\theta = 15$ °C isotherm at 200 (Kawai 1972). The water property during LM periods resembles the pure Kuroshio water well (Fig. 7c).

We next examine the sea surface current field to detect the ocean processes transporting the Kuroshio water into CAT. In October 2017 when the Kuroshio takes the LM path, a westward flow with a width of about 100 km bifurcates from the Kuroshio around 138° E, 34° N and passes through CAT (Fig. 8a). The westward Kuroshio bifurcation is also visible from a composite map during the LM periods (Fig. 8b). These analysis results indicate clearly that the heat transport associated with the westward Kuroshio bifurcation that occurs during the LM periods is the likely cause for inducing the coastal warming off the Tokai district.

4 Discussion and summary

Our analyses showed marked coastal warming off the Tokai district, Japan, during the LM periods. This is in sharp contrast to the previous recognition that a cool water pool is distributed broadly at the inshore region between the Kuroshio and the southern coast of the Tokai district. Large positive anomalies in both θ and S were evident of the Tokai district during the LM periods, not only at the sea surface but also below 300 m. We found that this inshore warm-salty water

was attributable to the westward Kuroshio bifurcation that occurs during the LM periods.

The width of the westward bifurcated flow is at most 100 km based on a rough estimate from satellite-derived altimeters (Fig. 8). It is, therefore, difficult to capture the detailed spatial and temporal features of the bifurcation from the existing altimeter data with a grid resolution of 25 km. The Surface Water and Ocean Topography (SWOT) (Fu and Ferrari 2008) wide-swath altimeter mission, which is planned to be launched in 2021, should in the future help us to capture smaller scales (about 10 km) and clarify the bifurcation processes. Ocean assimilation model has improved and progressed dramatically in recent years. These new assimilative data will also allow us to detect the bifurcation and to assess its influence on the coastal region south of Honshu quantitatively.

It is worth noting that an upward heat release is found due to the increased SST off the Tokai district. To obtain a further understanding of heat exchange between the ocean and atmosphere, here we examine the four components that comprise the NHF. As shown in Fig. 9, the results show that the NHF anomaly pattern reflects the latent heat flux predominantly and the sensible heat flux secondly in both the warm and cold seasons. Large upper ocean heat content (OHC) besides the increased SST is needed for the upward heat release in a form of turbulent heat flux. We examine the temporal evolution of OHC in the upper 300m (OHC_{300}) inside the CAT box. It is apparent that the OHC_{300} in LM periods is larger than that in non-LM periods every month,

especially in summer (Fig. 10). This implies the enhancement in upper OHC by the westward Kuroshio bifurcation in summer, leading to a significant influence on the overlying atmosphere via the upward heat release. The seasonal variation in the intensity of the Kuroshio bifurcation might be associated with that of the Kuroshio and the LM-induced cool water pool because they also tend to strengthen in summer (Sekine et al. 1985).

We detected the coastal warming from the spatially high-resolution MURSST data available after 2003 in Sect. 3. The LM occurred six times since 1965 (see shading periods in Fig. 1b); the last two events were the subject of this study. To examine the generality of our results, we investigate ocean and atmosphere patterns in the warm season of the six LM events. Here, we use the ERA5 SST data available from 1979. Although the resolution of the ERA5 atmospheric model is fixed from 1979 to present, the SST data prescribed at the lower boundary of the model has switched in September 2007. Specifically, the Hadley Centre Global Sea Ice and Sea Surface Temperature (HadISST) version2 data (HadISST2; Titchner and Rayner 2014) with a $1/4^\circ$ (longitude) \times $1/4^\circ$ (latitude) spatial resolution was used from January 1979 through August 2007 and the operational sea surface temperature and sea ice analysis (OSTIA)

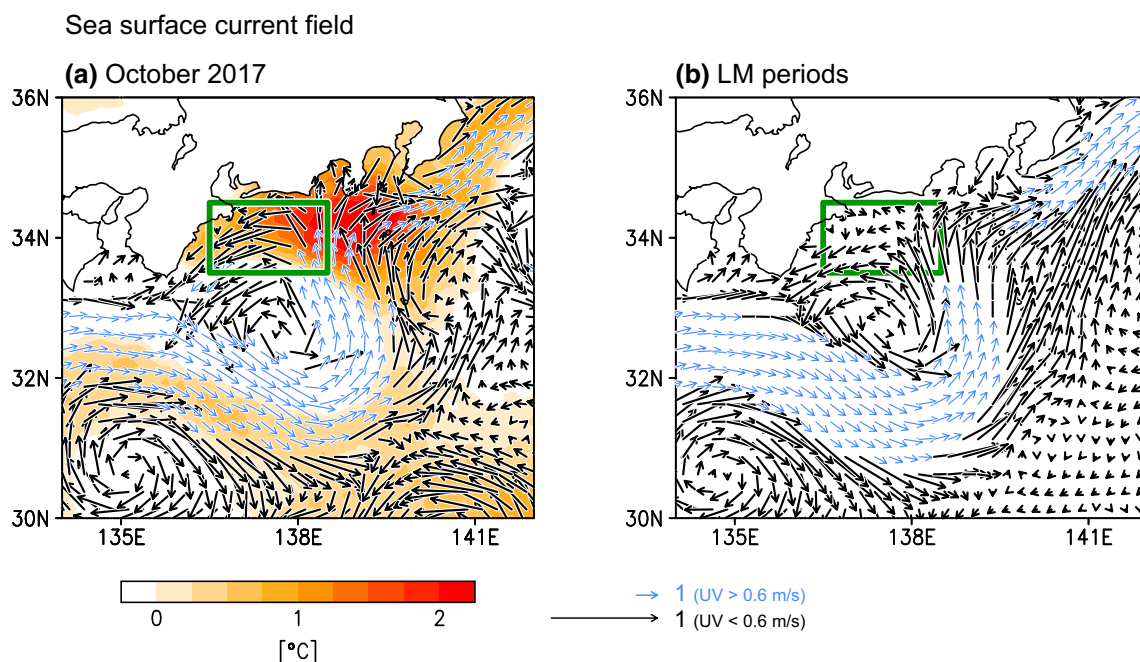
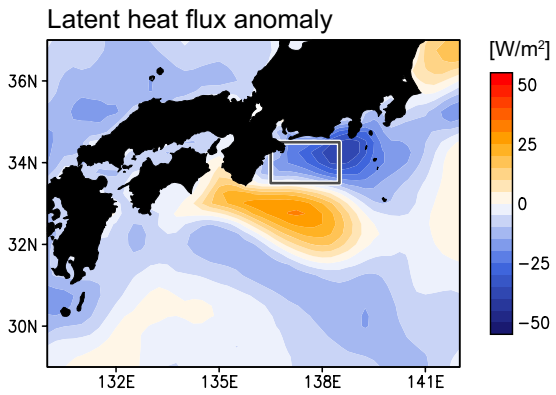
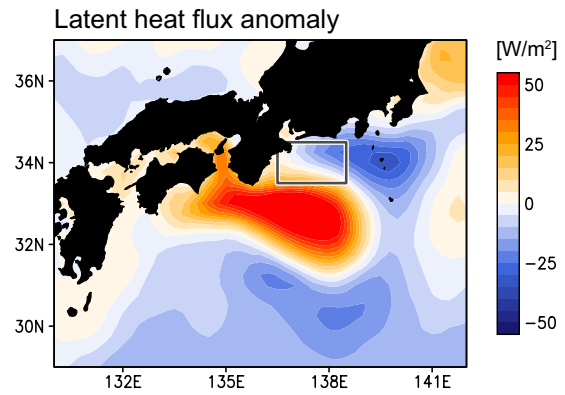


Fig. 8 **a** As in Fig. 2a, but for sea surface velocity vectors (arrows). Large velocity vectors ($> 0.6 \text{ m s}^{-1}$) are blue and rescaled. Green rectangle represents CAT. **b** As in **a**, but for a composite map during LM periods

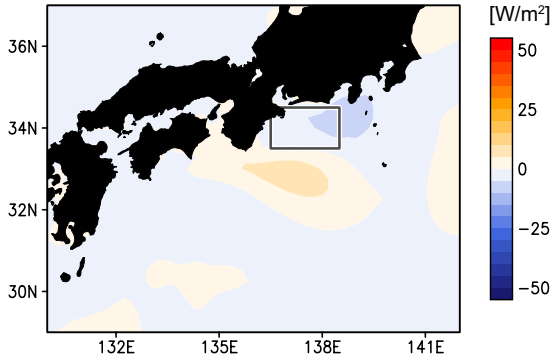
(a) Warm season during LM periods



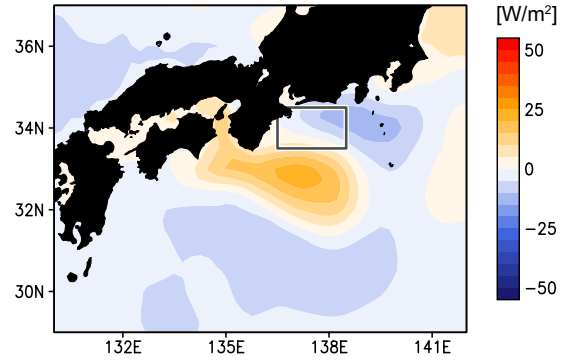
(b) Cold season during LM periods



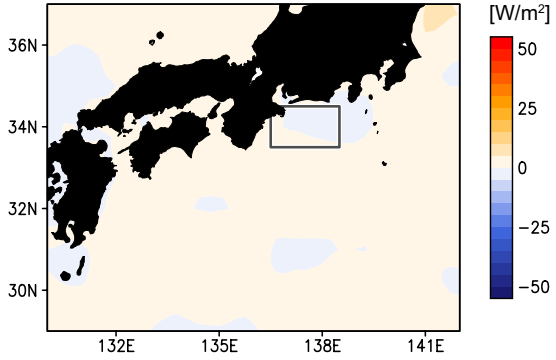
Sensible heat flux anomaly



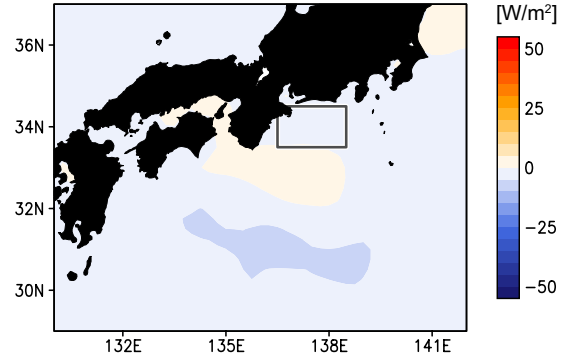
Sensible heat flux anomaly



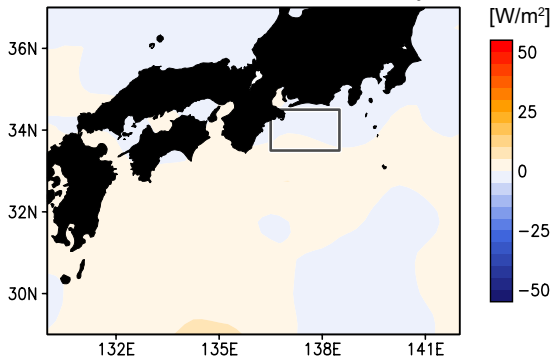
Net longwave radiation anomaly



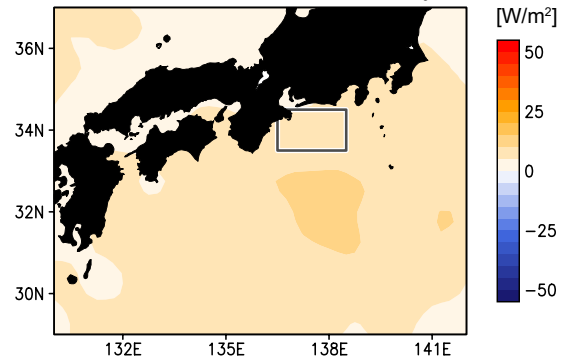
Net longwave radiation anomaly



Net shortwave radiation anomaly



Net shortwave radiation anomaly



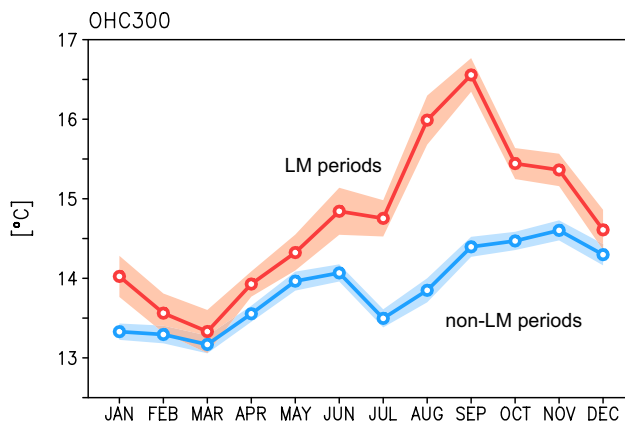


Fig. 10 Monthly time series of OHC_{300} in CAT during LM periods (red line) and non-LM periods (blue line), from archived temperature profiles. Shading denotes a confidence limit of 95%

data (Donlon et al. 2012) with a $1/20^\circ \times 1/20^\circ$ spatial resolution was used after September 2007. In the current LM, the high-resolution ERA5 SST shows a marked coastal warming (Fig. 11a), which is consistent with MURSST (Fig. 2b). The low-resolution SST data reveals a similar

warming pattern in the past five LMs (Figs. 12a, 13, 14, 15, 16a). The ERA5 data represents the coastal warming associated with the LM path throughout the data period, indicating the ERA5 atmospheric variables substantially reflects the coastal warming. In order to obtain further evidence for the coastal warming, we explore temperature anomaly in subsurface layer by using archived-temperature profiles. The coastal warming off the Tokai district at 200 m depth is evident in all LM events (Figs. 11b, 12, 13, 14, 15, 16, 17b); CAT in LM events is 1–2 °C warmer than that in non-LM periods (Figs. 11c, 12, 13, 14, 15, 16, 17c). We checked that almost identical results were obtained at other depths (100 m and 300 m) (not shown). In the six LM events, over the warmed CAT, the latent heat flux is released from ocean to atmosphere (Figs. 11d, 12, 13, 14, 15, 16, 17d) and the SAT is increased (Figs. 11e, 12, 13, 14, 15, 16, 17e). Although the SAT over Honshu, Japan, takes various anomalies every LM event (Figs. 11e, 12, 13, 14, 15, 16e and Figs. 11f, 12, 13, 14, 15, 16f) since the Japanese summer climate is influenced by many other factors such as the West-Asian Japan and Pacific Japan teleconnection patterns (Wakabayashi and Kawamura 2004; Tachibana et al. 2004) and heat waves (Imada et al. 2019),

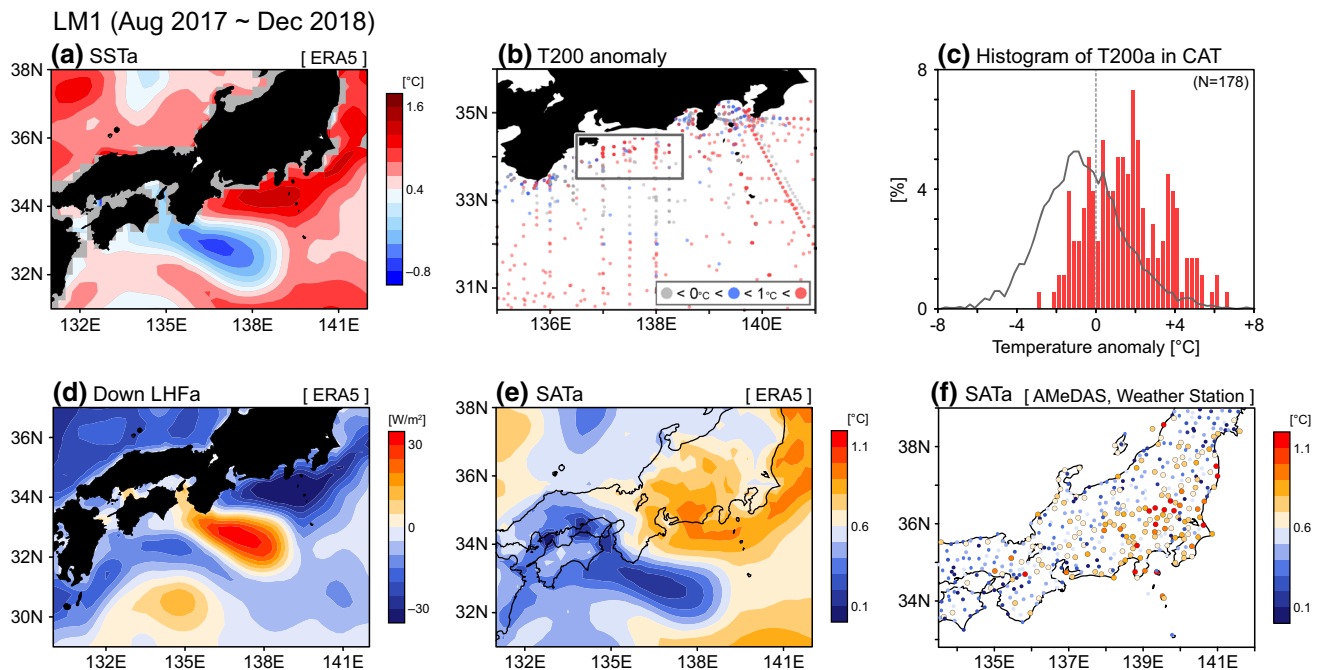


Fig. 11 Ocean and atmosphere patterns of warm season (May–October) during LM1 period. **a** Composite map of monthly SST anomaly, from ERA5 data; the value averaged within a region south of the Tokai [$32^\circ\text{--}35^\circ\text{N}$, $137^\circ\text{--}139^\circ\text{E}$] is the center of color bar. **b** Temperature anomaly at 200 m, from archived temperature profiles; we constructed the monthly temperature climatology averaged on a 1° (latitude) \times 1° (longitude) grid during non-LM periods since 1975, applying a method of Sugimoto et al. (2017a). Black rectangle represents

CAT. **c** Histogram of temperature anomaly at 200 m in CAT. Total number is shown in the upper right of panel. Black line indicates a histogram of temperature anomaly at 200 m of warm season during non-LM periods since 1975. **d** Composite map of monthly downward latent heat flux anomaly, from ERA5 data. **e** As in **a**, but for SAT anomaly, from ERA5 data. **f** As in **e**, but for weather station/AMeDAS data, with the same color scale with **e**

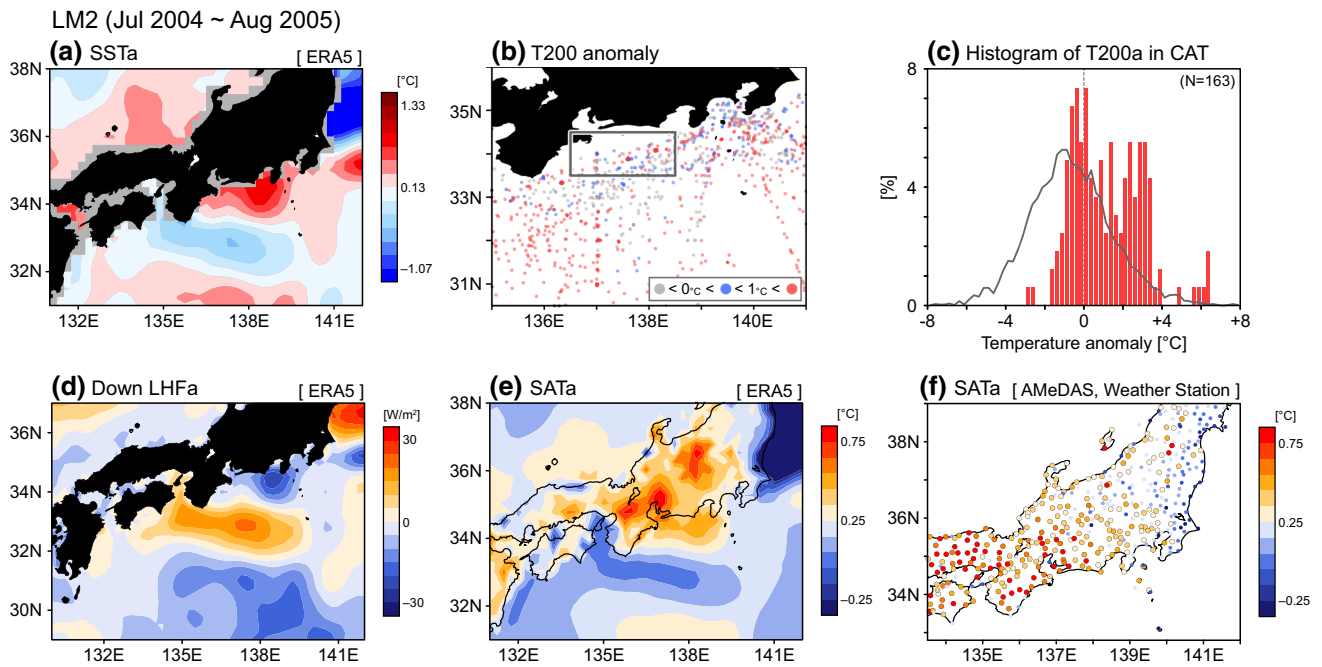


Fig. 12 As in Fig. 11, but for LM2 period

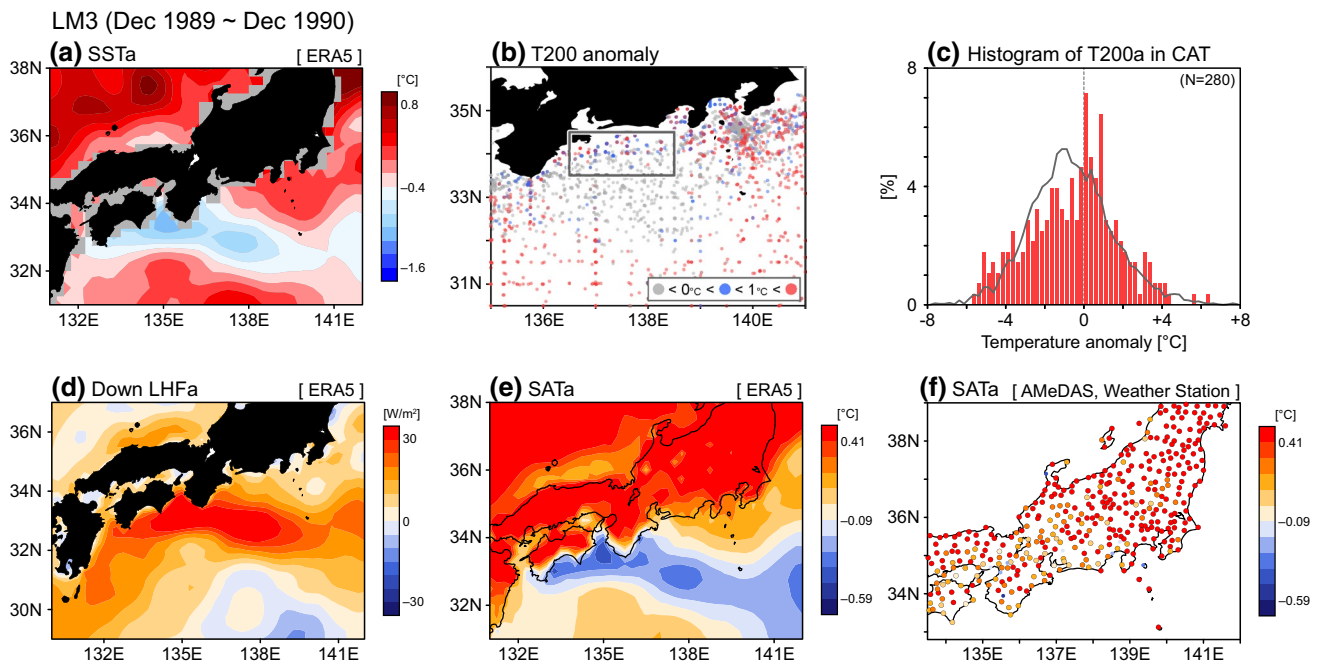


Fig. 13 As in Fig. 11, but for LM3 period

the warming around the Kanto-Tokai districts seems to be detected as a common feature of the LM (Fig. 17e, f). It is expected that the LM-induced coastal warming off the Tokai district exerts influence on the regional summer

climate around the Kanto-Tokai districts via the southerly winds that flow along the periphery of the western Pacific subtropical high, which are predominant over Japan in summer. Past studies have discussed influences of the

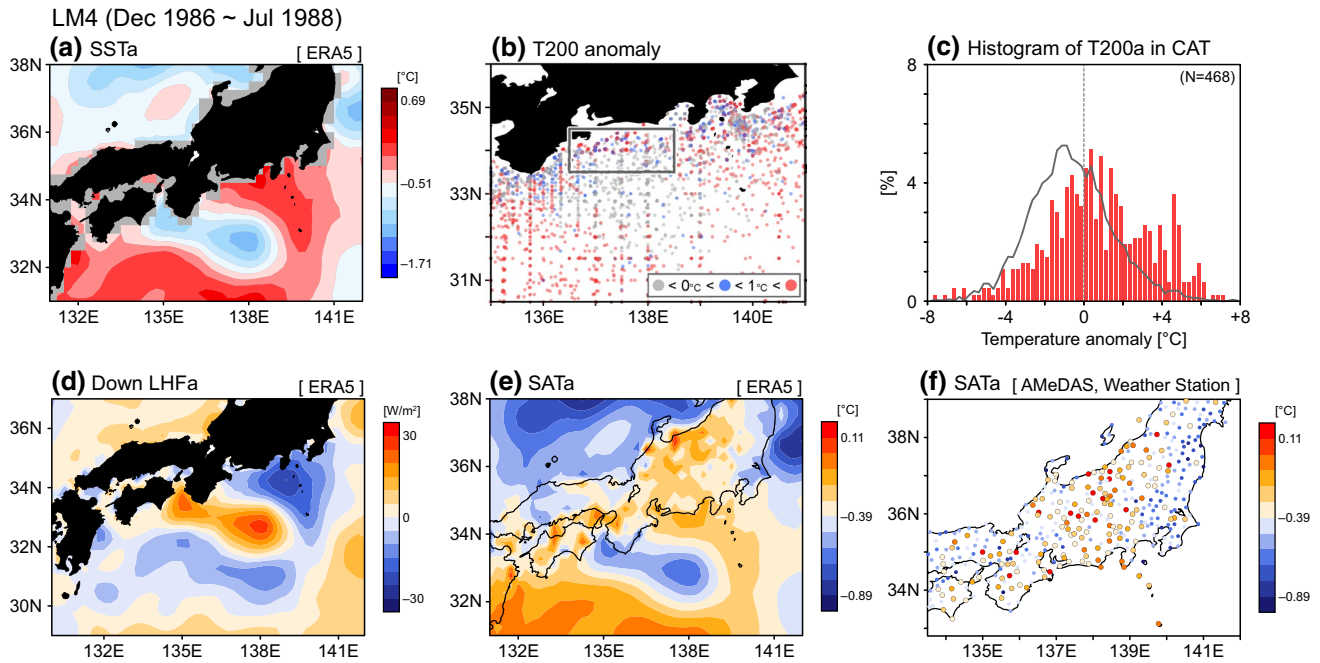


Fig. 14 As in Fig. 11, but for LM4 period

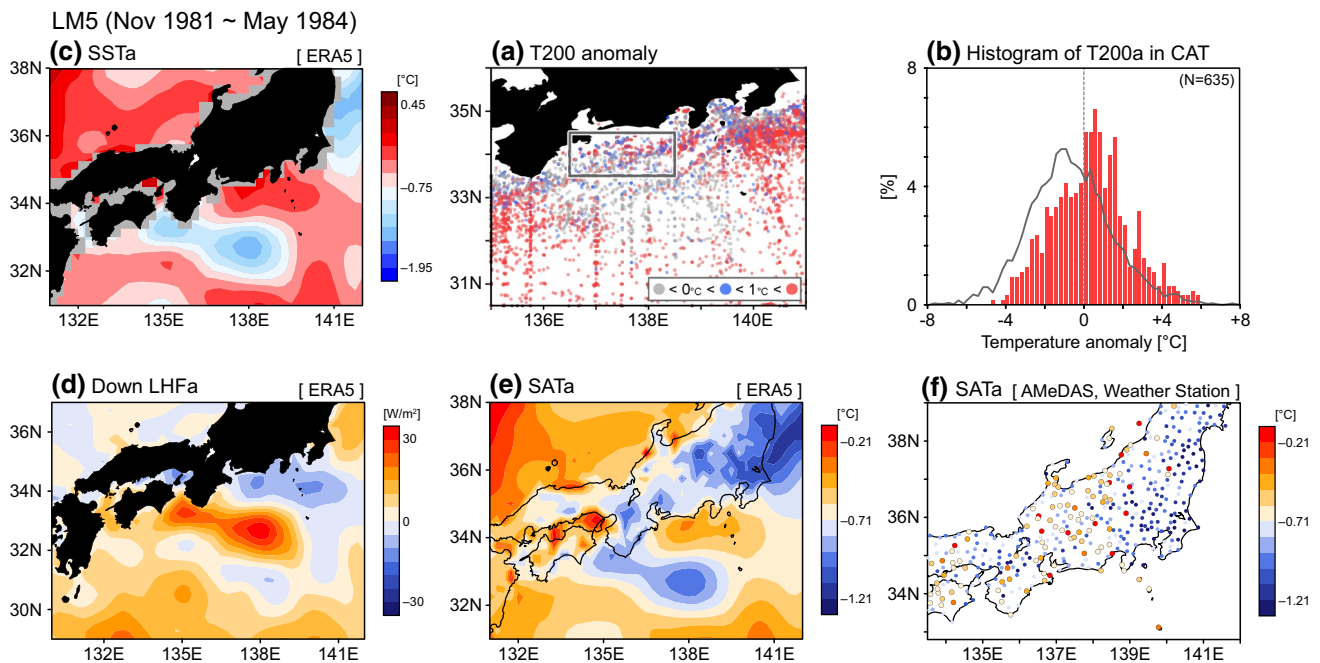


Fig. 15 As in Fig. 11, but for LM5 period

Kuroshio/KE on the atmosphere in winter (Xu et al. 2010; Tanimoto et al. 2011; Sugimoto and Hanawa 2011; Nakamura et al. 2012; Hayasaki et al. 2013; Sugimoto 2014; Ma et al. 2015, 2017; Masunaga et al. 2016; Sugimoto et al.

2017b; Kuwano-Yoshida and Minobe 2017) and in spring (Nonaka and Xie 2003; Miyama et al. 2012; Sasaki et al. 2012; Sasaki and Yamada 2018). Our results suggest that the summer coastal region will be a new scientific key area

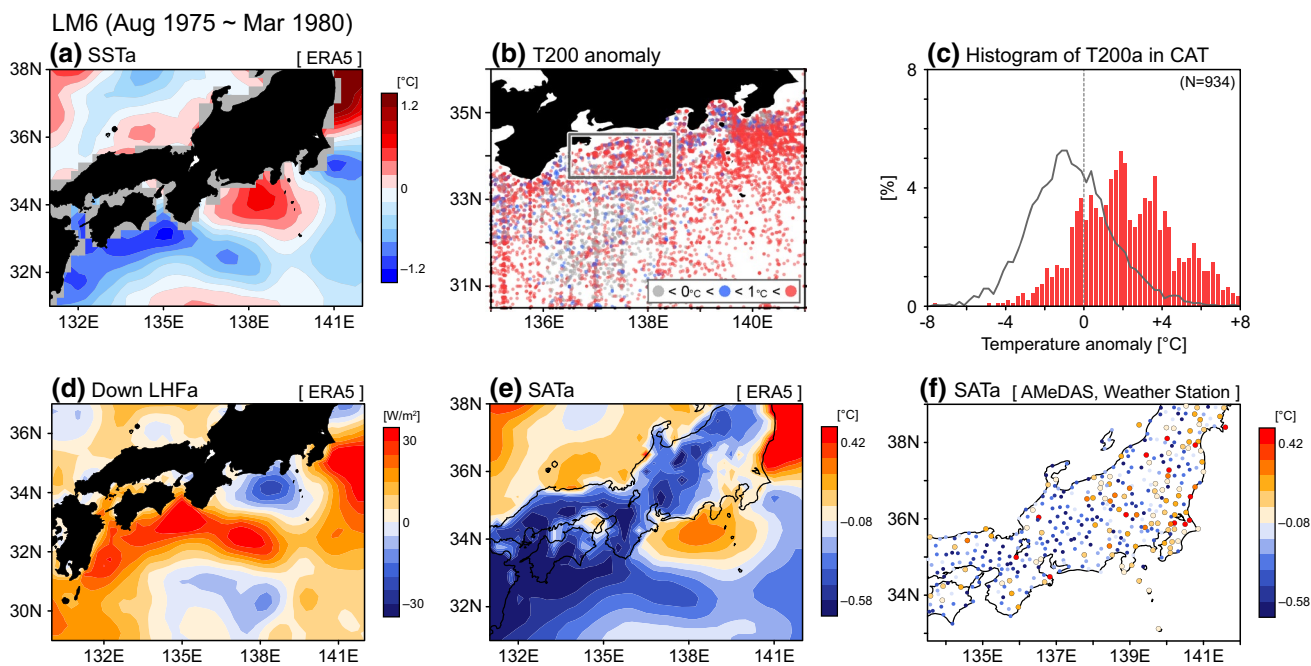


Fig. 16 As in Fig. 11, but for LM6 period

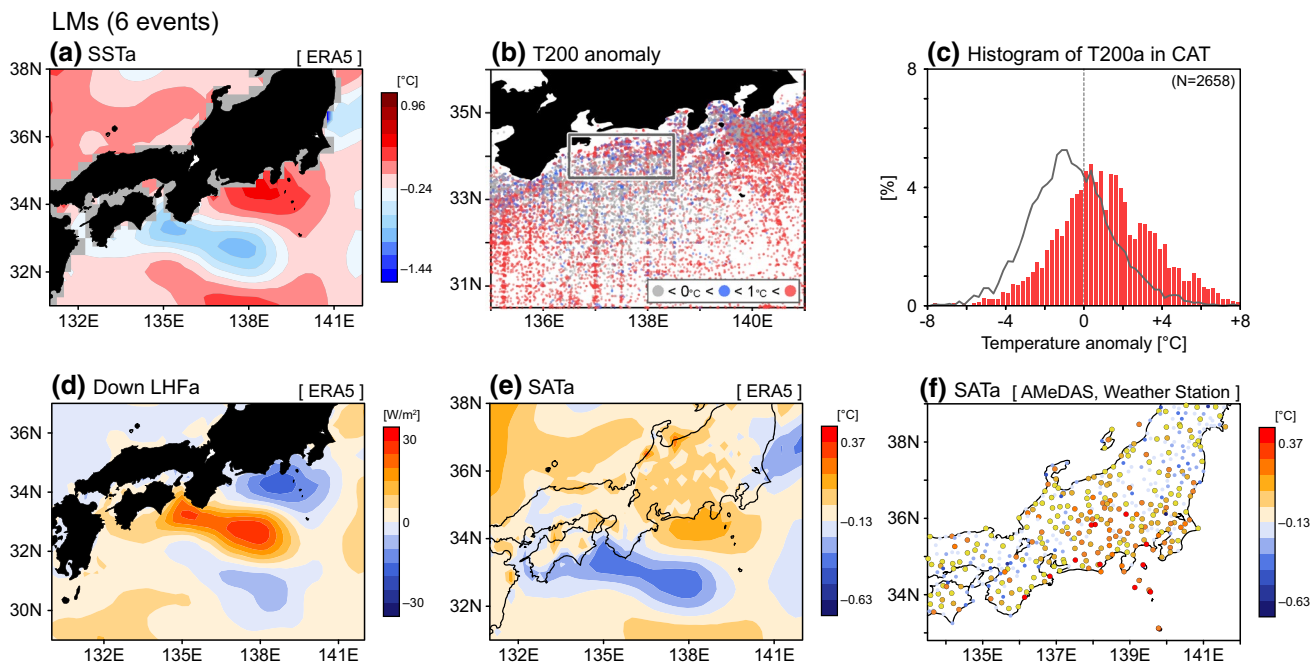


Fig. 17 As in Fig. 11, but for total 6 LM periods

for further understanding of the air-sea coupled system and regional climate.

Acknowledgements The authors thank Dr. Eitarou Oka and Dr. Niklas Schneider for valuable comments. The first author (SS) is supported by JSPS KAKENHI Grant numbers JP 18K03737 and 19H05704 and by the Japan Fisheries Research and Education Agency.

References

- Akima H (1970) A new method of interpolation and smooth curve fitting based on local procedures. *J Assoc Comput Mach* 17:589–602
- Argo Science Team (2001) Argo: the global array of profiling floats. In: Koblnsky CJ, Smith NR (eds) *Observing the oceans in the*

- 21st century. GODAE Proj Off Bur of Meteorol Press, Melbourne, pp 248–258
- Boyer TP et al (2018): World Ocean Database 2018. NOAA Atlas NESDIS 87, 207 pp. https://data.nodc.noaa.gov/woa/WOD/DOC/wod_intro.pdf
- Chin TM, Vazquez J, Armstrong E (2013) A multi-scale, high-resolution analysis of global sea surface temperature. *Algor Theor Basis Doc Vers 1* 200:13
- Copernicus Climate Change Service (C3S) (2017) ERA5: Fifth generation of ECMWF atmospheric reanalyses of the global climate, Copernicus Climate Change Service Climate Data Store (CDS). <https://cds.climate.copernicus.eu/cdsapp#!/home>. Accessed 25 Mar 2019
- Donlon CJ, Martin M, Stark J, Roberts-Jones J, Fiedler E, Wimmer W (2012) The operational sea surface temperature and sea ice analysis (OSTIA) system. *Remote Sens Environ* 116:140–158
- Fu LL, Ferrari R (2008) Observing oceanic submesoscale processes from space. *Eos Trans AGU* 89:488–488
- Gentemann CL, Fewings MR, García-Reyes M (2017) Satellite sea surface temperatures along the West Coast of the United States during the 2014–2016 northeast Pacific marine heat wave. *Geophys Res Lett* 44:312–319
- Hayasaki M, Kawamura R, Mori M, Watanabe M (2013) Response of extratropical cyclone activity to the Kuroshio large meander in northern winter. *Geophys Res Lett* 40:2851–2855
- Imada Y, Watanabe M, Kawase H, Shioyama H, Arai M (2019) The July 2018 high temperature event in Japan could not have happened without human-induced global warming. *SOLA* 15A:8–12
- Kasai A, Kimura S, Sugimoto T (1993) Warm water intrusion from the Kuroshio into the coastal areas south of Japan. *J Oceanogr* 49:607–624
- Kawabe M (1995) Variations of current path, velocity, and volume transport of the Kuroshio in relation with the large meander. *J Phys Oceanogr* 25:3103–3117
- Kawai H (1972) Hydrography of the Kuroshio extension. In: Stommel H, Yoshida K (eds) *Kuroshio: its physical Aspects*. University of Tokyo, Tokyo, pp 235–352
- Kuwano-Yoshida A, Minobe S (2017) Storm-track response to SST fronts in the Northwestern Pacific region in an AGCM. *J Clim* 30:1081–1102
- Ma X, Chang P, Saravanan R, Montuoro R (2015) Distant influence of Kuroshio eddies on North Pacific weather patterns? *Sci Rep* 5:17785. <https://doi.org/10.1038/srep17785>
- Ma X, Chang P, Saravanan R, Montuoro R, Nakamura H, Wu D (2017) Importance of resolving Kuroshio front and eddy influence in simulating the North Pacific storm track. *J Clim* 30:1861–1880
- Masunaga R, Nakamura H, Miyasaka T, Nishii K, Qiu B (2016) Interannual modulations of oceanic imprints on the wintertime atmospheric boundary layer under the changing dynamical regimes of the Kuroshio Extension. *J Clim* 29:3273–3296
- Maximenko N (2002) Index and composites of the Kuroshio meander south of Japan. *J Oceanogr* 58:639–649
- Miyama T, Nonaka M, Nakamura H, Kuwano-Yoshida A (2012) A striking early-summer event of a convective rainband persistent along the warm Kuroshio in the East China Sea. *Tellus A*. <https://doi.org/10.3402/tellusa.v64i0.18962>
- Murazaki K, Tsujino H, Motoi T, Kurihara K (2015) Influence of the Kuroshio Large Meander on the climate around Japan based on a regional climate model. *J Meteorol Soc Jpn* 93:161–179
- Nakamura H, Nishina A, Minobe S (2012) Response of storm tracks to bimodal Kuroshio path states south of Japan. *J Clim* 25:7772–7779
- Nakata H, Funakoshi S, Nakamura M (2000) Alternating dominance of postlarval sardine and anchovy caught by coastal fishery in relation to the Kuroshio meander in the Enshu-nada Sea. *Fish Oceanogr* 9:248–258
- Nonaka M, Xie SP (2003) Covariations of sea surface temperature and wind over the Kuroshio and its extension: evidence for ocean-to-atmosphere feedback. *J Clim* 16:1404–1413
- NRIFS (2005). Anomalous phenomena of fishing sea conditions related to the Kuroshio large meander (Central block). National Research Institute of Fisheries Science (NRIFS) website. https://nrifs.fra.affrc.go.jp/ResearchCenter/3_FOME/kuroshio/index.html. Accessed May 2005 (in Japanese)
- Oka E, Talley LD, Suga T (2007) Temporal variability of winter mixed layer in the mid- to high-latitude North Pacific. *J Oceanogr* 63:293–307
- Okada M (1977) Cold water mass off the Enshunada and mean sea level along the south coast of Japan. *Kaiyo-kagaku* 9:264–269 (in Japanese)
- Qiu B, Chen S, Hacker P (2004) Synoptic-scale air-sea flux forcing in the western North Pacific: Observations and their impact on SST and the mixed layer. *J Phys Oceanogr* 34:2148–2159
- Sasaki YN, Yamada Y (2018) Atmospheric response to interannual variability of sea surface temperature front in the East China Sea in early summer. *Clim Dyn* 51:2509–2522
- Sasaki YN, Minobe S, Asai T, Inatsu M (2012) Influence of the Kuroshio in the East China Sea on the early summer (Baiu) rain. *J Clim* 25:6627–6645
- Sekine Y, Ishii H, Toba Y (1985) Spin-up and spin-down processes of the large cold water mass of the Kuroshio south of Japan. *J Oceanogr Soc Jpn* 41:207–212
- Sugimoto S (2014) Influence of SST anomalies on winter turbulent heat fluxes in the eastern Kuroshio-Oyashio confluence region. *J Clim* 27:9349–9358
- Sugimoto S, Hanawa K (2011) Roles of SST anomalies on the wintertime turbulent heat fluxes in the Kuroshio-Oyashio confluence region: influences of warm eddies detached from the Kuroshio extension. *J Clim* 24:6551–6561
- Sugimoto S, Aono K, Fukui S (2017a) Local atmospheric response to warm mesoscale ocean eddies in the Kuroshio-Oyashio Confluence region. *Sci Rep* 7:11871. <https://doi.org/10.1038/s41598-017-12206-9>
- Sugimoto S, Hanawa K, Watanabe T, Suga T, Xie SP (2017b) Enhanced warming of the subtropical mode water in the North Pacific and North Atlantic. *Nature Climate Change* 7:656–658
- Tachibana Y, Iwamoto T, Ogi M, Watanabe Y (2004) Abnormal meridional temperature gradient and its relation to the Okhotsk high. *J Meteorol Soc Jpn* 82:1399–1415
- Tanimoto Y, Kanenari T, Tokinaga H, Xie SP (2011) Sea level pressure minimum along the Kuroshio and its extension. *J Clim* 24:4419–4434
- Titchner HA, Rayner NA (2014) The Met Office Hadley Centre sea ice and sea surface temperature data set, version 2: 1. Sea ice concentrations. *J Geophys Res Atmos* 119:2864–2889
- Usui N, Ishizaki S, Fujii Y, Tsujino H, Yasuda T, Kamachi M (2006) Meteorological Research Institute multivariate ocean variational estimation (MOVE) system: some early results. *Adv Space Res* 37:806–822
- Vazquez-Cuervo J, Dewitte B, Chin TM, Armstrong EM, Purca S, Alburquerque E (2013) An analysis of SST gradients off the Peruvian Coast: the impact of going to higher resolution. *Remote Sens Environ* 131:76–84
- Wakabayashi S, Kawamura R (2004) Extraction of major teleconnection pattern possibly associated with the anomalous summer climate in Japan. *J Meteorol Soc Jpn* 82:1577–1588
- Xu H, Tokinaga H, Xie SP (2010) Atmospheric effects of the Kuroshio large meander during 2004–05. *J Clim* 23:4704–4715